Microfluid Nanofluid (2016) 20:144
DOI 10.1007/s10404-016-1811-5

RESEARCH PAPER

A membrane-free micro-fluidic microbial fuel cell for rapid characterization of exoelectrogenic bacteria

Tran Chien Dang[1,2] · Yuan Yin[1] · Yangyang Yu[1] · Dinh-Tuan Phan[3] · Chun Yang[3] · Bin Cao[4] · Hao Song[5] · Yuejun Kang[6]

Received: 28 June 2016 / Accepted: 3 October 2016 / Published online: 11 October 2016

Abstract A membrane-free micro-fluidic microbial fuel cell (μMFC) has been developed in this work, in which the bacteria-mediated organic fuel oxidation process is physically separated from the proton exchange process that occurs between the laminar co-flows of anolyte and catholyte streams on a micro-fluidic chip. This new strategy aims to shelter exoelectrogenic bacteria in the anode chamber from the potential influence of the agents from the catholyte stream and enable much larger anode surface for bacteria adhesion in order to enhance the electron transfer efficiency. This μMFC reveals considerable difference in the relative open-circuit voltage produced by *Shewanella oneidensis* MR-1 and *Escherichia coli* DH5α, which can be established and stabilized within 2 h. This platform can be used for rapid characterization of the exoelectrogenic capability of various microorganisms or the development of a microbe-based electrochemical biosensor.

Keywords Microbial fuel cell · Micro-fluidics · Biosensor · Laminar flow · Exoelectrogen

1 Introduction

Microbial fuel cell (MFC) is a bioelectrochemical system using microorganisms as catalysts to decompose organic compounds and generate electric current. The electrons produced by bacteria during this process are transferred to the anode and flow through an external circuit to the cathode (Logan et al. 2006; Lovley 2008; Rabaey and Verstraete 2005). These electricity-generating microorganisms are also referred to as exoelectrogens, which have attracted extensive attention in recent years as an important alternative source for green and sustainable energy (Du

Tran Chien Dang and Yuan Yin have contributed equally to this work.

Electronic supplementary material The online version of this article (doi:10.1007/s10404-016-1811-5) contains supplementary material, which is available to authorized users.

✉ Bin Cao
bincao@ntu.edu.sg

✉ Hao Song
hsong@tju.edu.cn

✉ Yuejun Kang
yjkang@swu.edu.cn

[1] School of Chemical and Biomedical Engineering, Nanyang Technological University, Singapore, Singapore

[2] Advanced Environmental Biotechnology Centre, Nanyang Environment and Water Research Institute, Interdisciplinary Graduate School, Nanyang Technological University, Singapore, Singapore

[3] School of Mechanical and Aerospace Engineering, Nanyang Technological University, Singapore, Singapore

[4] School of Civil and Environmental Engineering, Nanyang Technological University, Singapore, Singapore

[5] Key Laboratory of Systems Bioengineering, SynBio Research Platform, Collaborative Innovation Centre of Chemical Science and Engineering, School of Chemical Engineering and Technology, Tianjin University, Tianjin 300072, China

[6] Institute for Clean Energy and Advanced Materials, Faculty of Materials and Energy, Southwest University, 2 Tiansheng Road, Beibei, Chongqing 400715, China

et al. 2007; Nor et al. 2015; Rabaey and Verstraete 2005; Wang et al. 2015). Many natural exoelectrogens have been reported, and genetically engineered exoelectrogens are under investigation for more efficient power generation (Kane et al. 2012; Mathuriya 2013; Voeikova et al. 2013; Wu et al. 2013).

As one of the major challenges in this field, it is highly laborious and time-consuming using conventional macro-scale MFCs for screening numerous genetically modified microbial strains to identify models with optimal stability and yield. To characterize these bacterial strains in a rapid fashion, some miniaturized MFCs have been conceived recently (Hou et al. 2010; Qian et al. 2011). A micro-fluidic MFC (μMFC) is usually featured by a large surface-area-to-volume ratio and thus enhanced affiliation between the bacteria and the anode, which can reach stabilized power output within less time while consuming less amount of carbon source compared to conventional MFCs (Wang et al. 2011; Yang et al. 2013). The proton exchange membrane (PEM) is extensively used in MFCs to separate cathode and anode. However, membrane fouling usually occurs in PEM, which compromises the performance of MFCs (Chae et al. 2008; Xu et al. 2012). Utilization of PEM also develops pH gradient between two electrodes, causing additional energy loss (ElMekawy et al. 2013). In addition, the incorporation of membrane in the micro-fluidic fuel cell further increases the manufacturing cost and complexity of the device (Wang and Su 2013). To address these issues, Wang and Su (2013) proposed a membrane-free MFC implementing a novel design that avoided using PEM. Specifically, the PEM-free MFC was achieved by taking advantage of the laminar co-flow generated in a micro-fluidic channel, which considerably improved the overall efficiency of characterizing the bacterial electrogenic activity. The laminar co-flow of the two electrolyte streams allows ionic conduction while reducing the mixing across the two co-flow streams (Ferrigno et al. 2002; Goulet and Kjeang 2014). However, maintaining a laminar co-flow poses a constraint on the width of the channel, limiting the effective contact area between the electrode and the bacteria. Moreover, because the anode is usually located nearby or in parallel with the co-flow region in most existing μMFCs, the constrained co-flow region limits the effective surface area of the anode and hence the electron transfer efficiency.

Herein, we present a μMFC on a chip that can effectively address the above major limitations of the existing membrane-free μMFCs. Specifically, two expanded reaction chambers are designed in the upstream before the catholyte and anolyte converge and form the laminar co-flow. This special design uses the upstream chambers for redox reactions, while maintaining the proton exchange process in the downstream co-flow region. This strategy aims to physically separate the proton exchange process from the bacteria-mediated oxidation process, so that the exoelectrogenic bacteria in the anode chamber can be sheltered from the influence of potential agents diffused from the catholyte stream. In addition, this strategy enables a much larger anode surface for bacteria adhesion in order to enhance the electron transfer efficiency and lower the system inner resistance (Du et al. 2007). A micro-stopper array is fabricated in the anode chamber to help retain the bacteria and slow down the local medium flow speed, which could provide a more amenable microenvironment for bacterial growth.

2 Materials and methods

2.1 Materials and reagents

The materials and chemical reagents are listed as follows. Polished silicon wafers, SU8 developer and SU8 photoresist were purchased from Microchem, USA. Sylgard 184 silicon elastomer kit was obtained from Dow Corning Inc., USA. Sodium lactate, NH_4Cl, KCl, Na_2HPO_4, Na_2SO_4, $MgSO_4{\cdot}7H_2O$, piperazine-*N*,*N*′-bis(2-ethanesulfonic acid) (PIPES), NaCl, $CaCl_2$, Na_2MoO_4, $CuCl_2{\cdot}2H_2O$, $FeCl_2{\cdot}4H_2O$, $MnCl_2{\cdot}4H_2O$, $CoCl_2{\cdot}4H_2O$, $ZnCl_2$, H_3BO_3, $NiSO_4{\cdot}6H_2O$, $Na_2SeO_3{\cdot}5H_2O$, $Na_2WO_4{\cdot}2H_2O$ and riboflavin were obtained from Sigma-Aldrich. Deionized (DI) water was collected from Millipore Synthesis A10 (Molsheim, France). *Shewanella oneidensis* MR-1 (ATCC 700550) was acquired from American Type Culture Collection (Manassas, VA), and *Escherichia coli* DH5α (DSM 6897) was obtained from the German Collection of Microorganisms and Cell Cultures (DSMZ) (Braunschweig, Germany).

2.2 Chip design and fabrication

Three types of μMFC chips were designed to compare their performance and identify the optimal design (Fig. 1a). The first one has a simple Y-shape. The second is with expanded cathode and anode chambers. The third is with micro-stoppers in the anode chamber. The purpose of including the expanded chambers and stoppers is to maximize the bacteria retention on the anode and increase the surface area of electrode for efficient electron transfer.

A glass substrate (1.5 in. × 3 in.) was used to pattern the electrodes. A layer of negative photoresist (SU8-3010) was spin-coated on the glass substrate and then exposed to UV irradiation through a film photomask. A 1.0-mm-wide pattern of photoresist (to separate anode and cathode) was formed on the glass substrate after rinsing in SU8 developer. A 200-nm layer of gold was deposited on the glass wafer by sputtering (coaxial magnetron sputter).

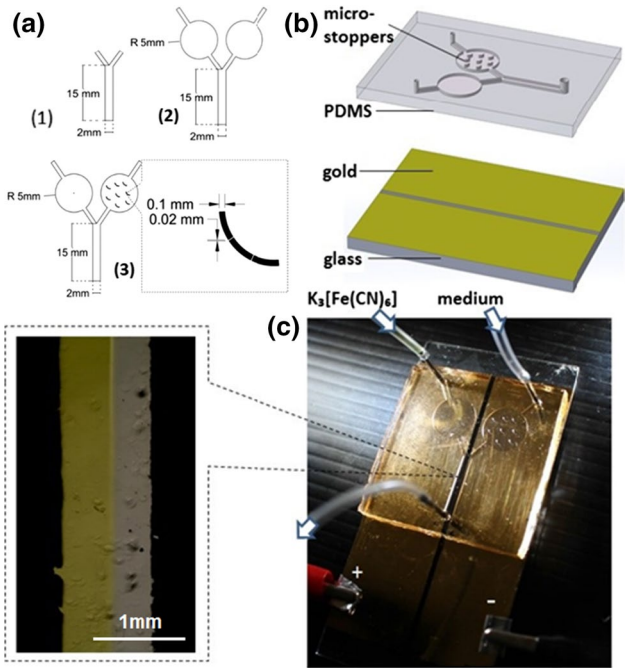

Fig. 1 Design and assembly of membrane-free μMFC. **a** Three types of μMFC chip designs for comparison: (*1*) Y-shape; (*2*) expanded cathode and anode chambers without micro-stoppers; and (*3*) micro-stoppers in the expanded anode chamber. **b** Schematic illustration of the major components of μMFC. **c** The image of an assembled μMFC. The gold electrodes were connected to a digital multimeter for OCV measurement. The enlarged *inset* shows the laminar co-flow in the downstream microchannel after electrolytes are pumped in. The *yellow* solution on the *left* is catholyte (color figure online)

The photoresist was then stripped by acetone. The polydimethylsiloxane (PDMS) micro-fluidic channels were fabricated following soft lithography method. A 3-in. silicon wafer was spin-coated with a negative photoresist (SU8-2075) at 2000 rpm for 120 s to achieve coating thickness of 100 μm. The wafer was then pre-baked on a hotplate at 65 °C for 5 min and at 95 °C for 20 min, followed by UV irradiation through a film photomask containing the pattern of microchannels. After UV exposure, the wafer was baked at 65 °C for 5 min and 95 °C for 10 min and then immersed in SU-8 developer with gentle shaking for 7 min for complete developing. A mixture of silicon elastomer base and curing agent at a mass ratio of 10:1 was cast onto the SU-8 mold and cured at 70 °C for 3 h. Then, the PDMS slab with designed channel structure was sliced and peeled off from the mold. Before assembling the parts, the PDMS chip and gold-patterned glass substrate were rinsed with DI water and autoclaved at 120 °C under 10 atm. for 20 min for sterilization. The PDMS chip was manually stacked onto the substrate with the microchannel aligned along the gap between two electrodes (Fig. 1c). A dual-syringe pump (KDS Legato 180) was used to infuse the anolyte and catholyte into the micro-chambers.

2.3 Data acquisition

A digital multimeter (3146A ESCORT) was used to measure the open-circuit voltage (OCV) produced by the μMFC. The gold electrodes were connected to the digital multimeter by electrical clips. An aluminum foil was placed between the gold electrode and the electrical clip to ensure close contact for electric conduction. Data were recorded at 2-min interval for totally 1–1.5 h until a stabilized output was achieved. The polarization curves and power curves of the system were measured using linear sweep voltammetry (LSV) at a scan rate of 1 mVs^{-1} over a range from open-circuit voltage to 0 mV. The LSV data were recorded using an Autolab PGSTAT 302 N potentiostat (Metrohm, the Netherlands) and NOVA 1.9 software. The internal resistance of the μMFCs was calculated based on the polarization curves (Fan et al. 2008). For the linear (ohmic) region of the polarization curves, the relationship between the external voltage (E) and the current (I) is expressed in the following equation.

$$E = E_b - R_{int}I \quad (1)$$

where E_b denotes the intercept of the linear (ohmic) region of the polarization curve with the voltage axis. R_{int} represents the internal resistance of the μMFC, which can be determined by linear fitting of the polarization curve.

2.4 Cell culture

Shewanella oneidensis MR-1 and *E. coli* DH5α were used as two model bacteria for this proof-of-concept study. The bacteria were cultured in standard Luria broth (LB) media under aerobic conditions at 30 °C for MR-1 and at 37 °C for DH5α under shaking speed of 200 rpm overnight, followed by another passage under the same condition for 8 h; 100 μL culture solution with an optical density (600 nm) between 0.6 and 0.7 was transferred to room temperature to ensure a consistent concentration throughout the experiments. The minimal medium contained 28 mM NH_4Cl, 1.34 mM KCl, 5 mM Na_2HPO4, 0.7 mM Na_2SO_4, 1 mM $MgSO_4{\cdot}7H_2O$, 20 mM PIPES, 52 mM NaCl, 0.2 mM $CaCl_2$, 5 mg/L $MnCl_2{\cdot}4H_2O$, 0.5 mg/L Na_2MoO_4, 0.02 mg/L $CuCl_2{\cdot}2H_2O$, 10 mg/L $FeCl_2{\cdot}4H_2O$, 3 mg/L $CoCl_2{\cdot}4H_2O$, 2 mg/L $ZnCl_2$, 0.2 mg/L H_3BO_3, 1 mg/L $NiSO_4{\cdot}6H_2O$, 0.06 mg/L $Na_2SeO_3{\cdot}5H_2O$ and 0.08 mg/L $Na_2WO_4{\cdot}2H_2O$ (Ding et al. 2014; Zachara et al. 1998). The lactate medium was prepared by adding 20 mM sodium lactate as the carbon source and 5 mg/L riboflavin as the electron shuttle mediator to the minimal medium. The fresh anolyte was prepared by mixing lactate medium solution, bacterial culture solution and 2 % LB solution at a volume ratio of 9:1:1. The fresh catholyte contained 50 mM potassium ferricyanide in buffered solution (pH 7.5).

2.5 Bacterial fixation and imaging

After operation for about 1.5 h, the μMFC was disassembled and rinsed with minimal medium. The adherent bacteria were fixed in 2 % glutaraldehyde solution overnight at 4 °C and then dehydrated by sequentially transferring through 50, 70, 90 and 100 % ethanol for 10 min in each solution and dried at 50 °C in a thermostatic oven for 2 h. Before imaging, the fixed samples were sputter-coated with platinum. Images were taken using a field emission scanning electron microscope (JSM-6700F). The bacteria adhered inside the PDMS anode chamber were imaged with an inverted microscope (Olympus IX71).

2.6 Statistical analysis

One-way analysis of variance (ANOVA) and Turkey honestly significant difference (HSD) test were used to statistically analyze the significant difference of OCV and signal-to-background ratio among three designs. Student's *t* test was used to analyze the significant difference of the OCV output between MR-1 and DH5α. The difference between data were considered statistically significant if the *p* value was <0.05.

3 Results and discussion

Rather than designing an MFC for power generation, this study was focused on the optimization of a μMFC for characterizing the exoelectrogenic capability of bacteria. Specifically, the performance of the μMFC was evaluated with two different bacterial models, namely *S. oneidensis* MR-1 and *E. coli* DH5α. The OCV of the μMFC was used as a simple and effective indicator to evaluate the exoelectrogenic capability of the particular bacterial strains (Logan et al. 2006).

The system was set up by infusing anolyte and catholyte into the μMFC at flow rate of 60 μL/min. The flow rate usually affects the laminar co-flow in a microchannel and the mixing rate of small molecules across the two-stream boundary (Choban et al. 2004). Under this applied flow rate, the Reynolds number (*Re*) in the co-flow region was <10. Therefore, a laminar co-flow was maintained to minimize the mixing of oxidation agent and other species from the catholyte stream with the anolyte stream. In the meantime, proton exchange was allowed across these two streams.

The background signals in Fig. 2a were the OCVs measured for the bacteria-free chips with three different designs as negative control. These background voltages were generated due to different redox potentials between the medium in anode chamber and the buffer in cathode

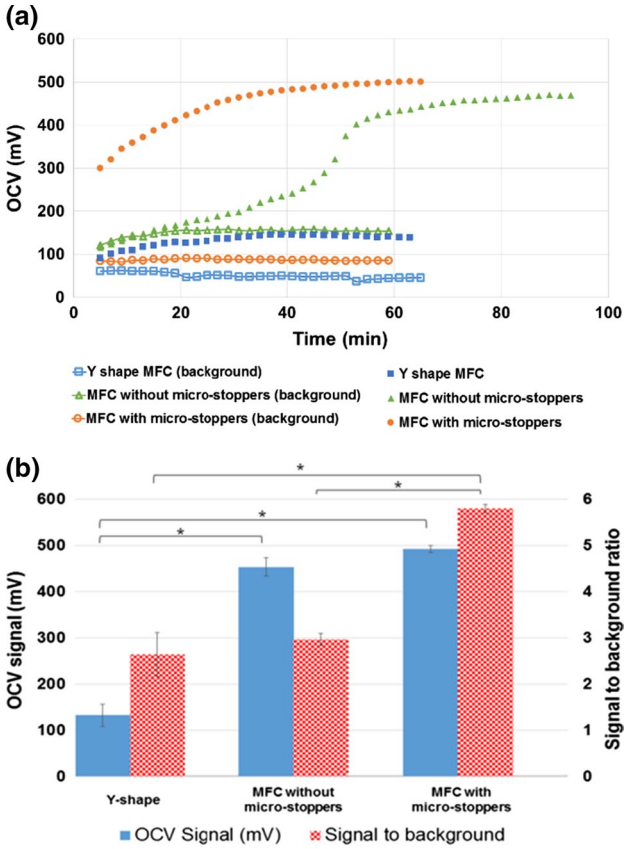

Fig. 2 Characterization of μMFCs. **a** Background OCVs and OCVs produced by MR-1 in three chip designs. **b** Average stabilized OCVs produced by MR-1 and the signal-to-background ratios. The data are shown as mean ± SD ($n = 3$). *p value <0.05 (Turkey HSD test) indicates significant difference between two groups

chamber (Logan et al. 2006), which needed to be considered to accurately evaluate the exoelectrogenic capability of the bacteria. The different background OCVs measured in three designs were due to the different μMFC configurations, including the surface area of electrodes and the fluid velocity distribution inside the chambers, which influenced the resultant redox potential. The experimental results indicated that the Y-shape μMFC with the smallest electrode area exhibited consistently the lowest background at 50 mV. For designs with expanded reaction chambers, the background OCV increased considerably to 155 mV, while the one with micro-stoppers in anode chamber reduced the background to a moderate level of 87 mV. This notable difference was due to the unique micro-stopper design. Although the micro-stoppers did not change the surface area of the electrode significantly, they increased the flow resistance and decreased the flow velocity in the anode chamber as shown by numerical simulation (Fig. S1, Supporting Information). As reported in the literature on laminar flow-based micro fuel cells (Choban et al. 2004; Sprague et al. 2009), the change of anolyte flow patterns

could affect the μMFC internal resistance to proton transport and hence the OCVs.

The laminar co-flow was developed immediately after the catholyte and bacteria-laden anolyte were introduced into the μMFC (Fig. 1c, inset). The measured OCV quickly adjusted and increased to a stabilized output (Fig. 2a). The time required to reach a stabilized output ranged from about 10 to 90 min, depending on the specific chip design and bacterial species. The μMFC with expanded reaction chambers typically required a longer time for output stabilization. In contrast, it usually takes a few days for conventional MFCs to reach stabilized output (Fan et al. 2012; Yu et al. 2011), while a few hours for many existing miniaturized MFCs (Qian et al. 2011). In addition, it was obvious that three different μMFC designs produced different levels of output OCV after stabilization (Fig. 2b). The two μMFCs with expanded reaction chambers (with and without micro-stoppers) generated significantly higher output OCV (at 492 ± 7.55 and 453 ± 19.97 mV, respectively) compared to the Y-shape design that had a final output of only 132 ± 23.33 mV (p value < 0.05), which implied that larger electrode surface area in the μMFC played an important role to enhance the total output OCV. Meanwhile, the μMFC with micro-stoppers produced higher OCV than the design without micro-stoppers, indicating that micro-stoppers enhanced the bacteria–electrode interaction and thereby increased the output OCV signal. On the other hand, the background OCV also increased considerably due to the enlarged electrode surface (Fig. 2a). Because the background OCV was not contributed by the bacteria, we measured the signal-to-background ratio (Fig. 2b) to evaluate the contribution solely by the bacteria, which showed significant difference (p value < 0.05) between the μMFC with (5.79 ± 0.09) and without (2.96 ± 0.13) micro-stoppers. For the Y-shape μMFC, however, the output OCV was considerably lower than the designs with expanded chambers (Fig. 2a, b) because it had much smaller surface area of the electrodes. Although the Y-shape μMFC produced the lowest background OCV, the considerably lower output OCV caused the lowest signal-to-background ratio. Therefore, μMFC with micro-stoppers produced the highest signal-to-background ratio among three different designs due to the unique micro-stopper feature, which reduced the background OCV while increasing the output OCV and thereby enhanced the overall sensitivity for exoelectrogenic bacteria screening.

Based on these observations, the μMFC with expanded reaction chambers and micro-stoppers exhibited the highest efficiency among three designs with regard to OCV generated by the exoelectrogens. We further measured and compared the raw OCVs produced by DH5α (Fig. S2, Supporting Information) and MR-1 (Fig. 2), respectively, using three different designs. The average OCVs produced

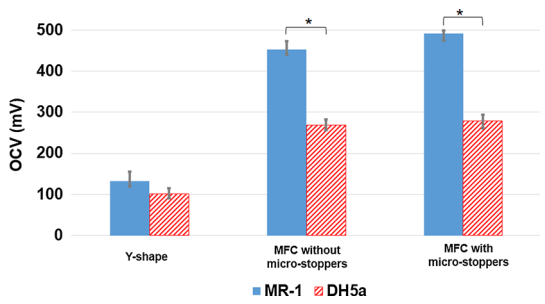

Fig. 3 Comparison of the stabilized OCVs produced by MR-1 and DH5α. The data are shown as mean ± SD. *p value <0.05 (Student's t test) indicates significant difference between two groups

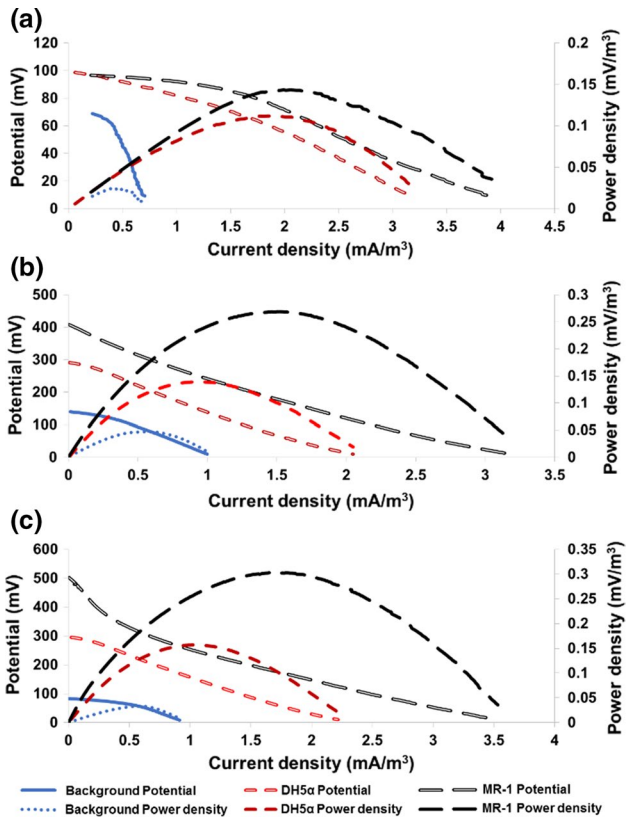

Fig. 4 Polarization curves obtained from three different designs using linear sweep voltammetry (LSV) methods at a scan rate of 1 mV/s. **a** Y-shape MFC; **b** μMFC without micro-stoppers; and **c** μMFC with micro-stoppers

by MR-1 and DH5α in three designs are shown in Fig. 3. According to the statistical analysis, it was evident that there was no significant difference between the OCV produced by two bacterial strains in the Y-shape design, while the OCV produced by MR-1 was significantly greater than that by DH5α in the other two designs (p value < 0.01). For the Y-shape μMFC, MR-1 generated 30 % higher OCV than DH5α. Meanwhile, the OCV produced by MR-1 was

Table 1 Current and power generation details of different designs

	Y-shape MFC		MFC without micro-stoppers		MFC with micro-stoppers	
	DH5α	MR-1	DH5α	MR-1	DH5α	MR-1
Anode chamber volume ($\times 10^{-9}$ m^3)	2.00	2.00	98.5	98.5	98.5	98.5
Projected anode area ($\times 10^{-5}$ m^2)	1.25	1.25	9.10	9.10	9.10	9.10
Maximum power (nW)	1.399	1.796	12.625	24.439	14.287	27.579
Maximum power density (volumetric) (W/m^3)	0.699	0.898	0.128	0.248	0.145	0.280
Maximum power density (by area) (mW/m^2)	0.112	0.144	0.139	0.269	0.157	0.303
Calculated internal resistance (MΩ)	2.91	2.58	1.76	1.28	1.65	1.13

67 % and 76 % higher than the OCV produced by DH5α in the μMFC with expanded chambers, without and with micro-stoppers, respectively. There are many prior studies that have investigated either DH5α (Qiao et al. 2007) or MR-1 (Qian et al. 2011) as the catalysts in various MFC devices. However, to the best of our knowledge, no prior study has characterized and compared the electrogenic capability of these two bacterial strains on the same platform. In the present study, MR-1 and DH5α exhibited different exoelectrogenic capabilities under the same condition. These results suggested that this μMFC could be used as an efficient tool for rapid analysis of different exoelectrogenic microorganisms.

The polarization curves and power output obtained for different designs and bacterial strains are shown in Fig. 4. It was observed that MR-1 outperformed DH5α in all three designs in terms of potential and power density. Typically, the power density initially increased to a maximum with the increase in current and then gradually decreased with further increase in current. Table 1 summarizes the major data of different μMFC designs and bacterial strains derived from the polarization curves (Fig. 4). The maximum power density by MR-1 was always greater than that by DH5α, which was consistent with the above results related to OCV. The maximum power density by area produced by both DH5α and MR-1 was highest on the μMFC with expanded chambers and micro-stoppers. However, for maximum power density by volume, the Y-shape μMFC exhibited the highest density among three designs, which was due to the fact that the Y-shape μMFC has the highest surface-area-to-volume ratio compared to the other two designs. The maximum power output of the μMFCs with expanded chambers using MR-1 was about 0.3 mW/m^2 (Table 1), which was much lower than that (1.5–6.25 mW/m^2) by other similar devices reported in the literature (Qian et al. 2009, 2011). In terms of internal resistance, the Y-shape μMFC showed the greatest resistance of 2.91 and 2.58 MΩ for DH5α and MR-1, respectively, while the μMFC with micro-stoppers showed the lowest internal resistance of 1.65 MΩ for DH5α and 1.13 MΩ for MR-1. Generally, high internal resistance was expected for μMFCs due to the small contact area between electrolytes and electrodes. The internal resistance of our device (1 ~ 3 MΩ) was much higher than those of other existing μMFCs (13–30 kΩ, Qian et al. 2009, 2011). This was due to the relatively short operation time of the proposed μMFCs (~1.5 h) compared to other μMFCs. Hence, the biofilm coverage on the anode surface was still low (Fig. 5a), which caused relatively higher resistance of the anode. Moreover, the distance between two electrodes in our current devices was 1.0 mm, which was much greater than that in other μMFCs using PEM membrane (~300 μm) (Qian et al. 2009, 2011) and hence increased the distance or internal resistance for proton transport. In fact, the lower power density as discussed above was attributed to the higher internal resistance in our device. Further improvement could be achieved by decreasing the gap size between two electrodes, which could shorten the proton transport distance and reduce the internal resistance. Nevertheless, this study demonstrated that the μMFC with expanded chambers and micro-stoppers was effective to improve the sensitivity compared to the previously reported Y-shape μMFC.

To verify the above findings, we also measured the OCVs produced by these two bacterial strains in a regular macroscale dual-chamber MFC (Fig. S3a, Supporting Information), while the culture conditions were maintained exactly same as in μMFCs. The results (Fig. S3b, Supporting Information) showed that both bacterial strains produced higher stabilized OCV (780 mV by MR-1, 454 mV by DH5α) in the macro-MFCs as compared to μMFCs (492 mV by MR-1, 280 mV by DH5α, Fig. 3), which was expected because the macro-MFC was featured by much greater contact area between the electrode and the bacteria, as well as a large proton exchange membrane. Meanwhile, MR-1 outperformed DH5α in terms of stabilized OCV in the macro-MFCs, which was consistent with the results obtained in μMFC. However, for both bacterial strains, it typically took several days for the macro-MFC to reach stabilized output (4 days for MR-1, 8 days for DH5α, Fig. S3b), whereas μMFC only took <2 h (Fig. 2a and Fig. S2). Considering the application for rapid screening the exoelectrogenic capability of various microorganisms or as a

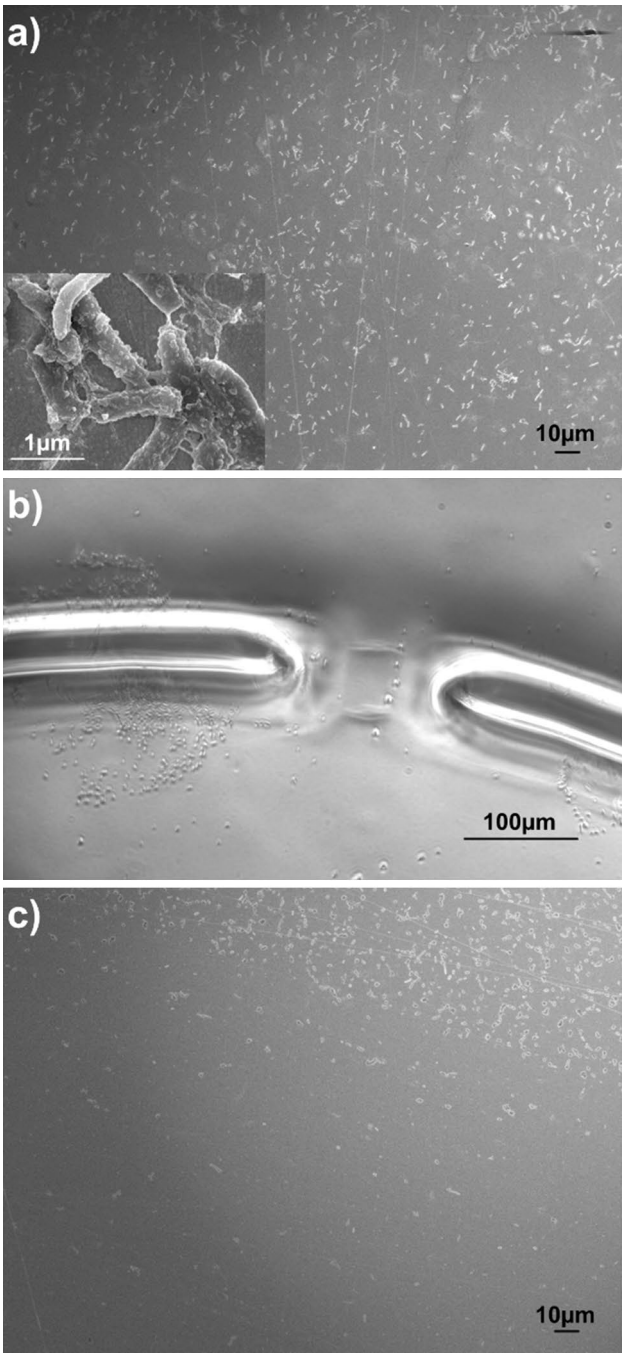

Fig. 5 **a** SEM image of MR-1 adhered on the gold anode of the μMFCs with micro-stoppers. *Inset* MR-1 forming aggregates on the gold substrate. **b** Optical contrast image of MR-1 bacteria retained near a micro-stopper. **c** SEM image of MR-1 adhered on the gold anode of the μMFC without micro-stoppers

microbe-based electrochemical biosensor, the proposed μMFC was obviously more advantageous with rapid analysis, much less reagent consumption and good sensitivity.

After analysis of the bacterial exoelectrogenic capability, the μMFCs with expanded reaction chambers were dissembled and the bacteria were fixed for visualization. The gold electrode and PDMS anode chamber were examined with a scanning electron microscope and a light microscope. Figure 5a shows the remaining MR-1 bacteria adhered on the gold electrode of the μMFCs with micro-stoppers. A closer examination (Fig. 5a enlarged inset) revealed that some bacterial aggregates started forming biofilm, which could enhance the exoelectrogenic activity of MR-1. The bacterial accumulation was also observed near the PDMS micro-stoppers (Fig. 5b), indicating that the stoppers had facilitated retaining the bacteria inside the anode chamber. In contrast, the MR-1 bacteria adhered very sparsely on the anode of the μMFC without micro-stoppers (Fig. 5c). Particularly, there was almost no bacteria adherent at the center of the chamber where the flow velocity reached the maximum (Fig. S1a, Supporting Information).

4 Conclusion

In summary, we have fabricated and compared three different designs of membrane-free micro-fluidic MFC as an efficient tool for rapid characterization of different exoelectrogenic microorganisms on a chip. It has been demonstrated that the μMFC with expanded cathode and anode reaction chambers and micro-patterned stoppers can enhance the bacteria–electrode affiliation and improve the electrogenic output considerably. Comparing the relative open-circuit voltages produced by MR-1 and DH5α, this device is able to effectively distinguish two bacterial strains with different exoelectrogenic capabilities, which can be further confirmed by the polarization and power curves. We believe that such devices could be used for more extensive applications in exoelectrogenic microbe-related environmental sensing and screening.

Acknowledgments This study was supported by a Sustainable Earth Office (SEO) Award at Nanyang Technological University (M408120000) funded to Y.K. and C.B. The PhD scholarship from the Interdisciplinary Graduate School at Nanyang Technological University is gratefully acknowledged by T.C.D.

References

Chae KJ, Choi M, Ajayi FF, Park W, Chang IS, Kim IS (2008) Mass transport through a proton exchange membrane (nafion) in microbial fuel cells. Energy Fuels 22:169–176. doi:10.1021/ef700308u

Choban ER, Markoski LJ, Wieckowski A, Kenis PJA (2004) Microfluidic fuel cell based on laminar flow. J Power Sources 128:54–60. doi:10.1016/j.jpowsour.2003.11.052

Ding Y, Peng N, Du Y, Ji L, Cao B (2014) Disruption of putrescine biosynthesis in *Shewanella oneidensis* enhances biofilm cohesiveness and performance in Cr(VI) immobilization. Appl Environ Microbiol 80:1498–1506. doi:10.1128/AEM.03461-13

Du Z, Li H, Gu T (2007) A state of the art review on microbial fuel cells: a promising technology for wastewater treatment and bioenergy. Biotechnol Adv 25:464–482. doi:10.1016/j.biotechadv.2007.05.004

ElMekawy A, Hegab HM, Dominguez-Benetton X, Pant D (2013) Internal resistance of microfluidic microbial fuel cell: challenges and potential opportunities. Bioresour Technol 142:672–682. doi:10.1016/j.biortech.2013.05.061

Fan Y, Sharbrough E, Liu H (2008) Quantification of the internal resistance distribution of microbial fuel cells. Environ Sci Technol 42:8101–8107. doi:10.1021/es801229j

Fan Y, Han S-K, Liu H (2012) Improved performance of CEA microbial fuel cells with increased reactor size. Energy Environ Sci 5:8273–8280. doi:10.1039/C2EE21964F

Ferrigno R, Stroock AD, Clark TD, Mayer M, Whitesides GM (2002) Membraneless vanadium redox fuel cell using laminar flow. J Am Chem Soc 124:12930–12931. doi:10.1021/ja020812q

Goulet M-A, Kjeang E (2014) Co-laminar flow cells for electrochemical energy conversion. J Power Sources 260:186–196. doi:10.1016/j.jpowsour.2014.03.009

Hou H, Ceylan CU, Li L, De Figueiredo P, Han A (2010) A microfluidic microbial fuel cell array for electrochemically-active microbe screening and analysis. In: 14th international conference on miniaturized systems for chemistry and life sciences 2010, MicroTAS 2010, pp 677–679

Kane AL, Bond DR, Gralnick JA (2012) Electrochemical analysis of *Shewanella oneidensis* engineered to bind gold electrodes. ACS Synth Biol 2:93–101. doi:10.1021/sb300042w

Logan BE et al (2006) Microbial fuel cells: methodology and technology. Environ Sci Technol 40:5181–5192

Lovley DR (2008) The microbe electric: conversion of organic matter to electricity. Curr Opin Biotechnol 19:564–571

Mathuriya AS (2013) Inoculum selection to enhance performance of a microbial fuel cell for electricity generation during wastewater treatment. Environ Technol 34:1957–1964

Nor MHM, Mubarak MFM, Elmi HSA, Ibrahim N, Wahab MFA, Ibrahim Z (2015) Bioelectricity generation in microbial fuel cell using natural microflora and isolated pure culture bacteria from anaerobic palm oil mill effluent sludge. Bioresour Technol 190:458–465. doi:10.1016/j.biortech.2015.02.103

Qian F, Baum M, Gu Q, Morse DE (2009) A 1.5 μL microbial fuel cell for on-chip bioelectricity generation. Lab Chip 9:3076–3081. doi:10.1039/B910586G

Qian F, He Z, Thelen MP, Li Y (2011) A microfluidic microbial fuel cell fabricated by soft lithography. Bioresour Technol 102:5836–5840

Qiao Y, Li CM, Bao S-J, Bao Q-L (2007) Carbon nanotube/polyaniline composite as anode material for microbial fuel cells. J Power Sources 170:79–84. doi:10.1016/j.jpowsour.2007.03.048

Rabaey K, Verstraete W (2005) Microbial fuel cells: novel biotechnology for energy generation. Trends Biotechnol 23:291–298

Sprague IB, Dutta P, Ha S (2009) Characterization of a membraneless direct-methanol micro fuel cell. Proc Inst Mech Eng Part A J Power Energy 223:799–808. doi:10.1243/09576509JPE724

Voeikova TA et al (2013) Intensification of bioelectricity generation in microbial fuel cells using *Shewanella oneidensis* MR-1 mutants with increased reducing activity. Microbiology 82:410–414

Wang H-Y, Su J-Y (2013) Membraneless microfluidic microbial fuel cell for rapid detection of electrochemical activity of microorganism. Bioresour Technol 145:271–274. doi:10.1016/j.biortech.2013.01.014

Wang H-Y, Bernarda A, Huang C-Y, Lee D-J, Chang J-S (2011) Micro-sized microbial fuel cell: a mini-review. Bioresour Technol 102:235–243. doi:10.1016/j.biortech.2010.07.007

Wang H, Park JD, Ren ZJ (2015) Practical energy harvesting for microbial fuel cells: a review. Environ Sci Technol 49:3267–3277. doi:10.1021/es5047765

Wu Y, Guan K, Wang Z, Xu B, Zhao F (2013) Isolation, identification and characterization of an electrogenic microalgae strain. PLoS One 8:e73442. doi:10.1371/journal.pone.0073442

Xu J, Sheng G-P, Luo H-W, Li W-W, Wang L-F, Yu H-Q (2012) Fouling of proton exchange membrane (PEM) deteriorates the performance of microbial fuel cell. Water Res 46:1817–1824. doi:10.1016/j.watres.2011.12.060

Yang J, Ghobadian S, Goodrich PJ, Montazami R, Hashemi N (2013) Miniaturized biological and electrochemical fuel cells: challenges and applications. Phys Chem Chem Phys 15:14147–14161. doi:10.1039/C3CP50804H

Yu Y-Y, Chen H-l, Yong Y-C, Kim D-H, Song H (2011) Conductive artificial biofilm dramatically enhances bioelectricity production in Shewanella-inoculated microbial fuel cells. Chem Commun 47:12825–12827. doi:10.1039/C1CC15874K

Zachara JM, Fredrickson JK, Li SM, Kennedy DW, Smith SC, Gassman PL (1998) Bacterial reduction of crystalline Fe^{3+} oxides in single phase suspensions and subsurface materials. Am Mineral 83:1426–1443